



The Effect of Polarization and Reaction Mixture on the Rh/YSZ Oxidation State During Ethylene Oxidation Studied by Near Ambient Pressure XPS

A. Katsaounis¹ · D. Teschner^{2,3} · S. Zafeiratos⁴

Published online: 24 October 2018

© Springer Science+Business Media, LLC, part of Springer Nature 2018

Abstract

In this study, near ambient pressure X-ray photoelectron spectroscopy (NAP-XPS) is applied to investigate an electrochemical cell consisting of a rhodium thin film catalyst supported on an yttria-stabilized zirconia (YSZ) solid electrolyte under various ethylene-oxygen reaction mixtures. The aim of the study is twofold: first to show how the surface oxidation state of the Rh catalyst is correlated with the reactants feed composition and the temperature, and second, to reveal the effect of the anodic polarization on the stability of Rh oxides and the implications on the electrochemical promotion of catalysis. It is clearly shown that even under reducing conditions part of the Rh electrode remains oxidized at temperatures up to 250 °C. Reduction of the oxide can take place by increasing the temperature under C₂H₄ excess, something which is not happening under oxidizing reaction mixtures. Moreover, anodic polarization, i.e. oxygen ion supply to the surface, facilitates reduction of oxidized Rh electrodes over a broad range of ethylene-oxygen reaction mixtures. Remarkably, under mildly reducing conditions a stable ultrathin Rh surface oxide film forms over metallic Rh. This surface Rh oxide film (RhO_x) is associated to higher cell currents, counterintuitive to the case of bulk Rh oxides (Rh₂O₃).

Keywords Electrochemical promotion of catalysis (EPOC) · Near ambient pressure X-ray photoelectron spectroscopy (NAP-XPS) · Rh oxide · Ethylene oxidation

1 Introduction

The electrochemical promotion of catalysis (EPOC) or non-faradaic electrochemical modification of catalytic activity (NEMCA), which was discovered in the 1980s by Vayenas et al. is an interdisciplinary phenomenon observed at the interface of catalysis and electrochemistry [1, 2]. EPOC allows for continuous in situ control of the coverage of

promoting species (Na^{δ+}, K^{δ+}, O^{δ-}) on the catalyst surface. It has been investigated extensively during the last 30 years for more than 100 catalytic reaction systems using a variety of metal catalysts (or conductive metal oxides), solid electrolytes and catalytic reactions [3–8]. In EPOC studies the conductive catalyst-electrode is in contact with an ionic conductor ceramic support and the catalyst is promoted by applying a current, or potential, between the catalyst film and a counter electrode. Numerous surface science and electrochemical techniques have shown that EPOC is due to an electrochemically controlled migration (reverse-spillover or backspillover) of promoting species, from the ionic or mixed ionic-electronic conductor-support to the gas exposed catalyst surface [3–10]. Upon application of a change, ΔU_{WR}, to the electrical potential, U_{WR}, of the catalyst (working electrode) with respect to a reference electrode, these backspillover species accompanied by their compensating charge in the metal, migrates to the metal-gas interface, creating an overall neutral double layer, termed as the effective double layer. This ion backspillover causes a catalyst work function change, ΔΦ, and accordingly a modification of the

✉ S. Zafeiratos
spiros.zafeiratos@unistra.fr

¹ Department of Chemical Engineering, University of Patras, GR26504 Patras, Greece

² Fritz-Haber-Institut der MPG, Faradayweg 4-6, 14195 Berlin, Germany

³ Max Planck Institute for Chemical Energy Conversion, Stiftstraße 34-36, 45470 Mülheim an der Ruhr, Germany

⁴ Institut de Chimie et Procédés pour l'Énergie, l'Environnement et la Santé (ICPEES), ECPM, UMR 7515 CNRS-Université de Strasbourg, 25, rue Becquerel, 67087 Strasbourg Cedex 02, France

chemisorptive bond strengths of the reactants and intermediates [3, 8]. Parameters such as the coverage of the spillover species, the equilibrium surface coverage of the spillover species and the charge of the spillover species can play an important role on the relation between the work function and the overpotential, ΔU_{WR} , of the catalyst/electrode [11]. In the case of O^{2-} (YSZ) and Na^+ ($\beta''\text{-Al}_2\text{O}_3$) spillover, over a wide range of conditions, there is a proportional relationship between the work function and the electrode potential change, i.e. $\Delta\Phi = e\Delta U_{\text{WR}}$ [3–8, 11]. In some cases, the promoting species can even change the oxidation state of the catalyst [3, 12–14]. Thus, both catalytic activity and selectivity can be effected in a pronounced, reversible, and, to some extent, predictable manner [3, 6]. The close connection between EPOC, classical chemical promotion and metal support interaction (MSI) with ionically conducting supports has been established by a variety of techniques [3, 4, 8, 15–18].

The reaction of ethylene oxidation to CO_2 on rhodium-based catalysts exhibits an extremely effective electrochemical promotion effect and therefore has been extensively studied in previous years [12–14, 19, 20]. The pronounced electrochemical promotion of Rh, was rationalized by the dependence of the reaction rate on the Rh oxidation state and particularly by the electrochemical stabilization of the active reduced form of Rh [12, 13, 19, 20]. The above conclusions were based on the measurements of the catalyst's potential as a function of the variations in the reactive gas mixture composition and the reaction temperature. In particular, under open circuit conditions (without current or potential application) as the oxygen partial pressure in the reaction mixture was increasing the reaction rate was increasing as well. At a critical gas composition an abrupt drop in reaction rate was observed followed by a parallel increase in the catalyst potential. This effect was attributed to Rh oxidation. When an anodic current or potential was applied to the Rh electrode (electropromoted conditions) the drop in the reaction rate was shifted to higher oxygen partial pressures [12, 13, 19, 20]. This was taken as a first indication that the anodic polarization (i.e. oxygen ion supply to the catalytic surface) helps to maintain Rh in the metallic state at higher oxygen partial pressures. It has been reported that the transition from a reduced to an oxidized surface and vice versa, is determined by the temperature, the applied potential and the oxygen partial pressure [12–14, 19, 20].

X-ray photoelectron spectroscopy (XPS) due to its high surface sensitivity is an ideal tool to analyse the topmost layers of the electrode. In addition, the chemical specificity of the technique not only allows elemental identification but also provides an assessment of the oxidation state of the electrode. In the pioneer work of the groups of Vayenas and Ladas [1], this technique was used for the first time to investigate in situ the effect of electrochemical promotion

on Pt catalysts interfaced with YSZ. However, conventional XPS spectrometers operate under vacuum conditions, which practically exclude the possibility to study the electrochemical promotion under relevant gas phase reaction mixtures [21]. The reinvention and significant development of XPS spectrometers able to operate at the mbar pressure regime (hereafter near ambient pressure XPS, NAP-XPS), can give a significant push in the comprehension of electrochemical promotion effects, since it allows in situ characterization of the catalyst/electrode state during the electrochemical promotion [22, 23]. To the best of our knowledge, so far NAP-XPS has been used only once by Imbihl and co-workers to study the electrochemical promotion of ethylene oxidation over a bimetallic Pt–Ag/YSZ catalyst [24]. However, it is still challenging to carry out a reliable kinetic study under NAP-XPS measurement conditions. This is due to the particularities of the NAP-XPS cell reactor (i.e. large volume of the chamber, relatively low partial pressures of the reactants, etc.) and the mass-transfer controlled conditions which are dominated in the system. Moreover, it is known that meaningful (i.e. kinetically controlled) catalytic data can only be obtained under conditions where the second Damköhler number (Da_{II}) is much smaller than unity [2, 25].

Here we report on a NAP-XPS experiment coupled with electrochemical measurements, to investigate a rhodium thin film catalyst supported on an YSZ solid electrolyte during ethylene oxidation. The main question we will try to address here is how the surface oxidation state of Rh catalysts can be correlated with the feed composition of the reactants and the electrochemical characteristics of the cell, under closed and open circuit conditions.

2 Experimental

The sample consists of a porous rhodium catalytic film, also serving as the working electrode, applied on 8 mol% YSZ electrolyte with a gold electrode on the opposite site acting as a counter electrode (this configuration is hereafter referred as electrochemical cell). Gold was used as the counter electrode as in many previous EPOC studies, due to its relatively inert catalytic properties. Both electrodes were deposited on YSZ by DC magnetron sputtering using high-pure argon as sputtering gas and pure Rh (99.99%) and Au (99.99%) as sputtering targets. The discharge characteristics have been controlled using a DC power supply. The sputtering chamber was evacuated to a base pressure of 7×10^{-7} Torr and then fed with argon gas at 100 sccm flow resulting in 4.5 mTorr chamber pressure during the deposition process. The substrate temperature was kept stable during the deposition at 50 °C. During all depositions, the substrate was placed 5.5 cm away from the target, which was found to result in good uniformity of the produced films. The sputtering

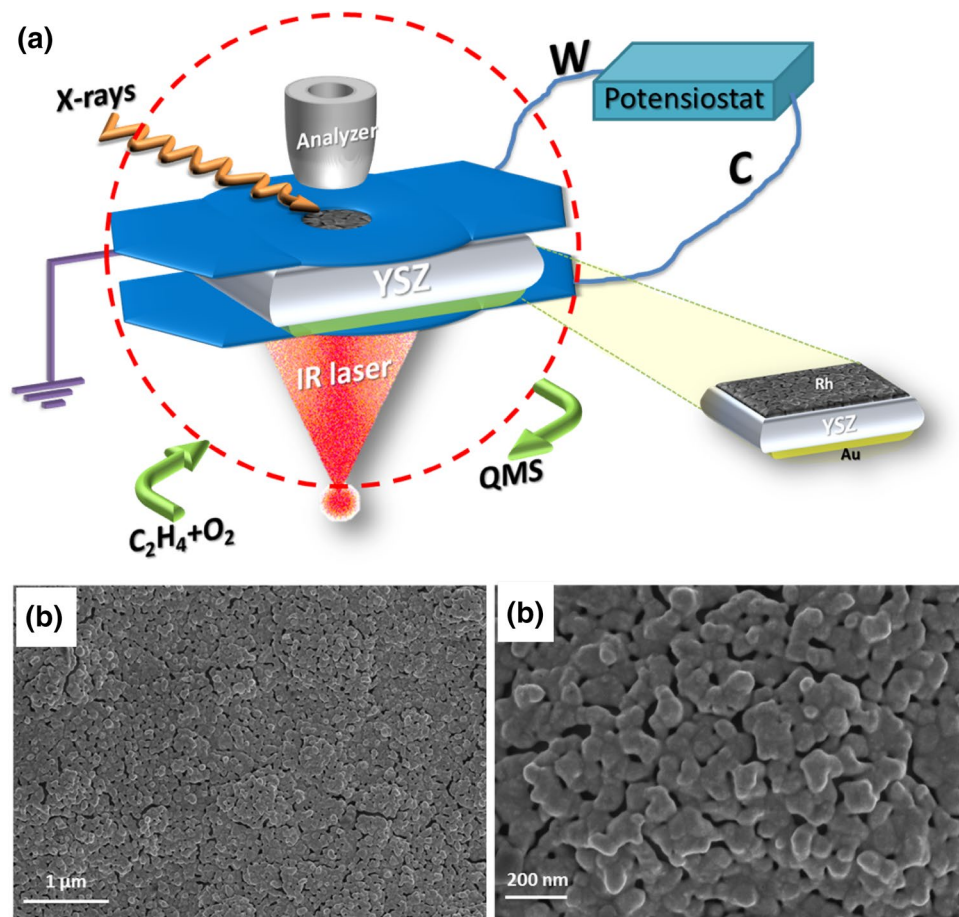
conditions were the following: direct current (dc) mode with a discharge of 350 V, argon pressure of 0.5 Pa. Under these conditions the deposition rate was 0.10–0.15 nm s⁻¹. The film thickness of the sputtered-deposited rhodium and gold films was < 40 nm.

The described experiments were performed at the ISSS beamline at BESSY II Helmholtz-Zentrum in Berlin, in a setup described in detail elsewhere [26]. The mounting layout of the electrochemical cell for the combined NAP-XPS/electrochemical characterization was similar to those described in earlier studies [27, 28]. In brief, cells of about 5 × 5 mm² area were mounted between two stainless steel clamps acting as the current collectors. NAP-XPS measurements were recorded through a 4 mm diameter hole at the cover clamp. The rear clamp was heated using an IR-laser and the temperature was measured by a K-type thermocouple attached to the Rh electrode. The laser heating is homogeneous in an area of 5 × 5 mm², therefore the temperature distribution is considered uniform in the overall measured cell area. In this setup the two sides of the cell are exposed to the same gas mixture, which corresponds to previously reported experiments on a single chamber reactor [14]. A schematic representation of the cell configuration inside the NAP-XPS chamber is given in Fig. 1a.

The gas flow into the reaction cell was controlled by pre-calibrated mass flow controllers and the gas phase composition was monitored on line by a differentially pumped quadrupole mass spectrometer (QMS), which was connected to the experimental cell through a leak valve. The QMS signal changes of the gases of interest were very low as compared to the relevant QMS background signal in the chamber and thus did not allow calculating in a reliable way the enhancement ratio due to the applied potential. The low QMS signal can be explained by the low pressure working conditions combined by the small catalyst exposed area and the relatively high reactor/XPS chamber volume (around 10 lt). Due to mass transfer limitations, the above experimental conditions unfortunately didn't allow us a meaningful kinetic study of the reaction.

The experiment was performed in several cycles on samples which were fragments of the same catalytic specimen. Prior to any reaction cycle, the sample was treated in oxidative (0.3 mbar O₂ at 500 °C) environments. The aim of this pretreatment was to refresh the surface and eliminate possible carbon deposits, as confirmed by the C1s XPS spectrum. The potential difference was applied directly between the working (W) and counter (C) electrodes without the use of a reference

Fig. 1 a Schematic representation of the cell configuration inside the NAP-XPS chamber. Top view SEM images of the Rh electrode surface after NAP-XPS measurements in **b** low magnification and **c** high magnification images



electrode. The W electrode (Rh film) was connected to the ground (i.e. $U_W = 0$) in order to avoid influence of the bias to the photoelectron peaks' binding energies. Therefore, the counter electrode (Au film) was biased -1.5 eV with respect to Rh in order to attain a total applied potential $U_{WC} = +1.5$ V. Under these conditions oxygen ions from the YSZ electrolyte migrate towards the metal gas interface of Rh. Experiments under open circuit (OC) and closed (1.5 V) circuit (CC) conditions were carried out consecutively on the same sample but in two separate experimental sequences. In particular, first the partial pressure ratio of the reactants (hereafter $R = p_{(C_2H_4)}/p_{(O_2)}$) was varied between 0 and 9 in a fixed total pressure of 0.3 mbar under OC conditions. In a consequent CC experiment, after refreshing in O_2 , a potential of 1.5 V was applied between the Rh working and the Au counter electrodes and the gas phase conditions were varied similar to the OC experiments. The open circuit potential, U_{WC}^o , (during OC experiments) and the current flow, i_{wc} , (during CC experiments), were measured using a computer controlled μ Autolab potentiostat/galvanostat, in conjunction with the NAP-XPS spectra.

The stability of the surface during the NAP-XPS measurements was verified by recording the Rh 3d spectrum at the beginning and at the end of the measurement cycles. Unless otherwise specified, the presented NAP-XPS spectra were acquired after 20 min equilibration in the gas mixture. Spectra were collected using appropriately selected photon energies, resulting in photoelectrons with two characteristic kinetic energies (180 and 590 eV), which give an estimated information depth for Rh of 1.4 and 2.9 nm respectively [29]. Samples did not exhibit any electrostatic charging under the employed experimental conditions and the binding energies are referred to the Fermi edge of the grounded spectrometer without scale correction. A Shirley background subtraction was used to estimate the peak areas and the quantitative calculations were performed taking into account the photon flux at the applied energy and the photo-ionization cross-sections dependence of the atomic subshells [30]. The oxide film thickness was estimated by a simplified formula described previously [31]:

$$d = \lambda \ln \left(\frac{I_{RhOx}}{I_{Rh}} + 1 \right) \quad (1)$$

where d is the Rh oxide film thickness, λ the inelastic mean free path of the photoelectrons and I_{RhOx} and I_{Rh} the measured XPS peak intensities of the oxide and metallic Rh components, respectively.

Finally, the surface morphology was inspected by scanning electron microscopy (SEM) using a Zeiss GeminiSEM 500 microscope.

3 Results and Discussion

3.1 The Morphology of the Rh Electrode

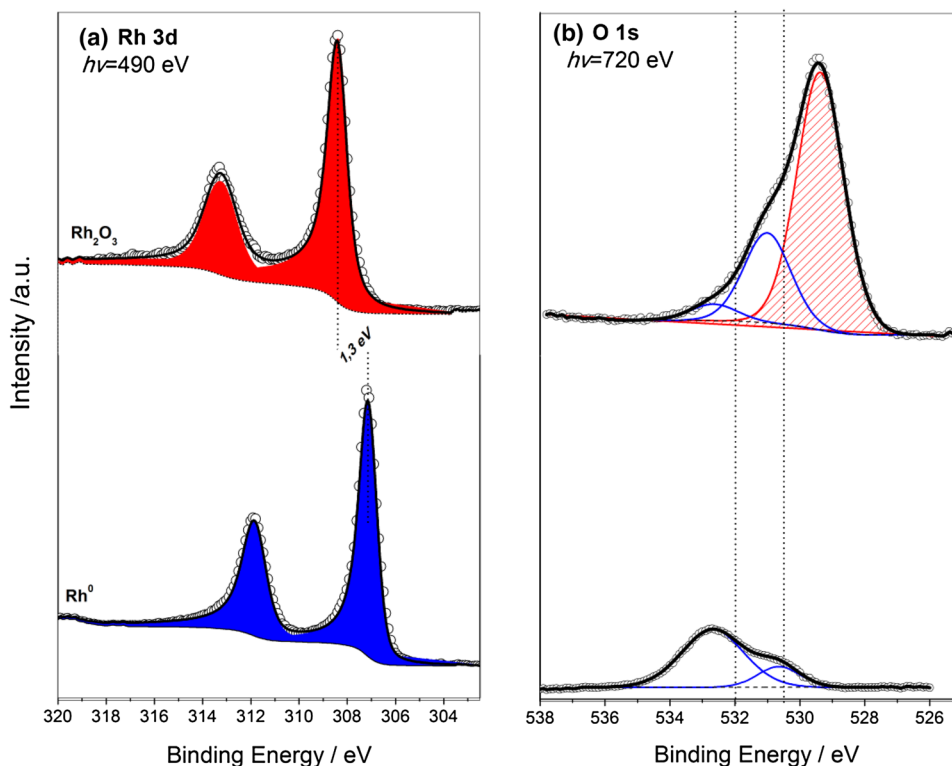
Figure 1b, c shows top view scanning electron microscopy images of the Rh film electrode on YSZ taken after the NAP-XPS experiments. The sample has been treated in the NAP-XPS chamber under various gas atmospheres and temperatures up to 500 °C for about 17 h. It can be observed that the Rh layer remains quite porous, which suggests that the YSZ support is accessible through these holes during our mbar pressure experiments. Please note that the porous morphology of the film enhances the access of the reactants and the three-phase boundary (tpb) length. It should be also mentioned that SEM images reveal a continuous metal film indicating a catalytic surface with high electrical conductivity which is very important in EPOC studies.

3.2 NAP-XPS Characterization of Thermally Oxidized and Reduced Rh Electrode

Initially the Rh electrode was oxidized at 500 °C in 0.3 mbar O_2 atmosphere for about 1 h in order to remove carbon residuals and to record reference spectra of the fully oxidized electrode. Consequently, the temperature was lowered to 400 °C and the O_2 atmosphere was replaced by 0.3 mbar H_2 , where reference spectra of the reduced electrode were recorded after 45 min. The Rh 3d spectra of oxidized and reduced electrodes recorded at the aforementioned conditions are shown in Fig. 2a. The Rh 3d peak is composed of two components due to Rh 3d_{5/2} and Rh 3d_{3/2} peak splitting. The peaks have an asymmetric peak profile. The best fitting of the Rh 3d_{5/2} is obtained by using a Doniach–Šunjić (DS) peak profile with asymmetry indexes $\alpha = 0.076$ and 0.098 for the metallic and oxidized Rh states respectively. The binding energy (BE) of the Rh 3d_{5/2} at 307.15 eV for the reduced electrode is consistent with the values reported for metallic rhodium [32–37]. The Rh 3d_{5/2} peak of the oxidized electrode is shifted by +1.3 eV to 308.45 eV as compared to the metal. The Rh 3d_{5/2} BE of different Rh-oxide components has been summarized previously in [36, 37]. According to these reports, the BEs of stoichiometric Rh_2O_3 and RhO_2 bulk oxides are shifted to higher BEs by about 1.2 and 2.2 eV respectively, as compared to the metallic Rh. Therefore, the 1.3 ± 0.1 eV shift of Rh 3d spectra measured in our study indicates the formation of bulk Rh_2O_3 on the electrode under the employed oxidation conditions.

The O 1s spectrum of oxidized Rh electrode plotted in Fig. 2b consists of a main peak at 529.4 eV and two

Fig. 2 **a** Rh 3d and **b** O 1s NAP-XPS spectra recorded in O₂ (top) and H₂ (down) atmospheres using 490 eV and 720 eV photon energies, respectively. Open circles are measured data and full lines are mathematical fit. The vertical lines in Fig. 2b indicate the expected BEs of O 1s peak due to the YSZ support



additional components shifted by 1.5 and 3 eV towards higher BEs. The peak at 529.4 eV is attributed to lattice oxygen species in bulk Rh₂O₃ [33, 34], while the higher BE O 1s peaks are related to a convolution of various species including adsorbed hydroxyl groups, defect sites [33, 34] and oxygen from the YSZ support accessible through the cracks of the film [23, 38]. The O/Rh ratio was ca. 2.4, while if only the area of the component at 529.4 eV is considered, this ratio drops to 1.6, close to the expected Rh₂O₃ stoichiometry (1.5). However, the quantitative interpretation of the O 1s spectra is not straightforward since it is critically influenced by uncertainties of the O 1s peak deconvolution procedure and the accurate determination of the sensitivity factors of the two elements. For this reason, we avoid to draw any conclusion about the stoichiometry of rhodium oxides based on the XPS peak intensity ratios. In the case of the reduced Rh electrode the intensity of O 1s peak drops considerably, while as expected the peak at 529.4 eV due to Rh₂O₃ disappears. However, some oxygen species at BEs 530.7 and 532.5 eV are still present in the O 1s spectrum as shown Fig. 2b. Please note that typically the O 1s peak of pure YSZ consists of a main component at 530.5 and a shoulder around 532.0 [21, 38, 39] (indicated by the dotted vertical lines in Fig. 2b). Therefore the O 1s spectrum of the reduced electrode shown Fig. 2b cannot be attributed entirely to the YSZ support but most probably also contains residual adsorbed species and potentially O-containing impurities. However, given that several

oxygen species appear within this narrow BE region, is very difficult to unambiguously define the exact origin of these species.

3.3 The Redox Effect of the Reaction Mixture Composition as a Function of Temperature

Rh/YSZ electrodes, pre-reduced in H₂ were subjected in heat treatments under oxidative (R = 0.2) and reducing (R = 3.6) reactant mixtures in order to investigate the effect of the reaction mixture composition on the oxidation state of Rh electrode. The temperature rise follows a liner ramp (rate 10 °C/min), while Rh 3d spectra were recorded in real time as a function of temperature every 12 °C (spectra acquisition time 20 s). The evolution of Rh oxidation state during temperature ramping was not abrupt but gradual allowing us to detect partial oxidized Rh electrode state. A characteristic example of Rh 3d spectrum recorded on a partially oxidized electrode is shown in Fig. 3. The spectrum displays the two characteristic Rh 3d doublets of metallic and oxidized Rh species. The fitting of the Rh 3d spectrum was performed using peak profiles (peak shapes) of fully reduced and oxidized Rh electrodes measured at the same spectrometer. The overall Rh 3d spectrum can be accurately reproduced by the appropriate linear combination of the oxidized and reduced Rh 3d spectra, shown in Fig. 2a, only if the BE the oxidized Rh peak is shifted (towards lower values) as compared to the reference Rh₂O₃ spectra. In particular, the BE of the

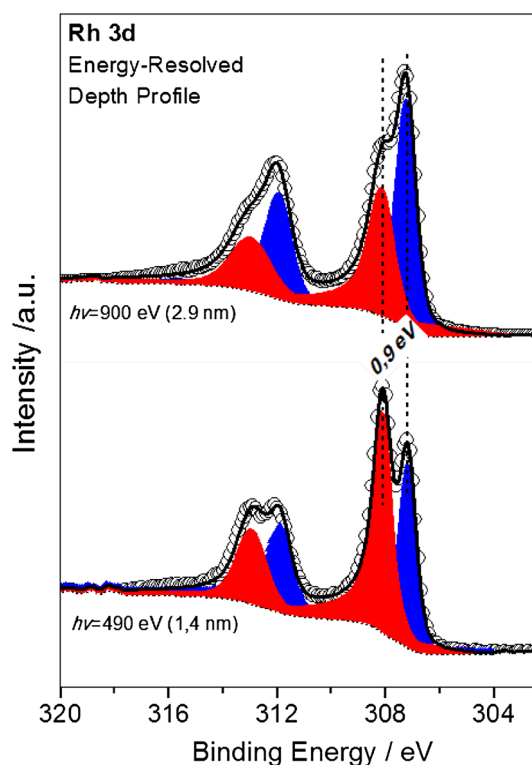


Fig. 3 Rh 3d spectra recorded at 400 °C in $p_{(\text{C}_2\text{H}_4)}/p_{(\text{O}_2)} = 0.2$ mixture at OC using two different photon energies and thus two analysis depths. Open circles are measured data and full lines are mathematical fit. The vertical lines are present as eye guide

oxide peak is located at 308.1 ± 0.1 eV, thus shifted only by 0.9 ± 0.1 eV with respect to metallic Rh. This shift is significantly lower than that of the reference Rh_2O_3 (1.3 eV) measured at the same experimental setup (see Fig. 2a). This finding indicates differences in the chemical environment of the Rh atoms in partially oxidized electrode not only as compared to the bulk Rh_2O_3 but also to any other bulk Rh oxides (please note that the RhO_2 peak is shifted even further to higher BE). On the other hand, previous theoretical and experimental studies has assigned Rh 3d peak shifts of the same magnitude (0.8 eV) to the formation of ultrathin surface oxide films on metallic Rh [37, 40].

In order to validate the assignment of the oxidized Rh component to a surface oxide, we performed energy dependent NAP-XPS measurements as shown in Fig. 3. We recall that by changing the energy of excitation ($h\nu$) one can select the desired surface sensitivity of the XPS method, which allows differentiation between surface and subsurface species [41]. This approach, usually referred as energy-resolved depth profiling, was performed here for the Rh 3d peak using two photon energies which correspond to an estimated maximum analysis depths of 1.4 and 2.9 nm. A simple comparison of the two spectra plotted in Fig. 3 shows a relative increase of the metallic Rh component with increasing the

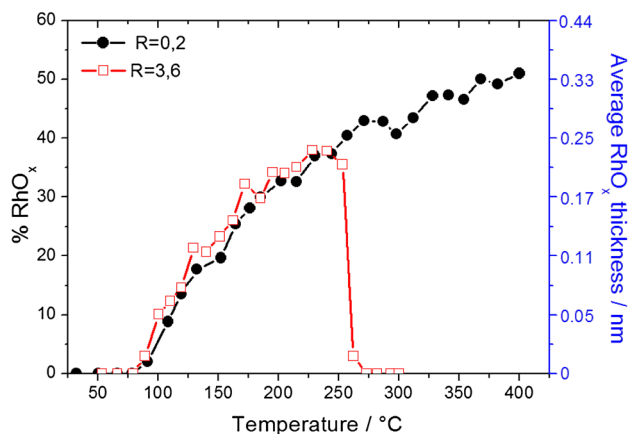


Fig. 4 The evolution of RhO_x to the overall Rh 3d NAP-XPS peak ($h\nu = 490$ eV) as a function of temperature recorded at OC in two $p_{(\text{C}_2\text{H}_4)}/p_{(\text{O}_2)}$ reaction mixtures at 0.3 mbar. Prior to the gas mixture introduction the Rh electrode was reduced in situ in H_2

photon energy. This observation indicates that the oxidized Rh is formed on the surface of the electrode, while metallic Rh is located underneath the oxide.

Both, the BE assignment and the depth profiling measurements suggest the formation of a low-dimensional oxide film on the surface of Rh electrode under the employed reaction conditions. The spectroscopic characteristics of this film resemble very much previous reports for ultrathin Rh-oxides preceding the growth of bulk Rh_2O_3 [34 and references therein]. The structure of this surface oxide consists of an O–Rh–O trilayer which resembles more the bulk RhO_2 termination instead of Rh_2O_3 [32, 40]. However, the electronic structure of the oxide film depends on several factors including thickness, changes in the local stoichiometry, defect sites, surrounding environment etc. [42], thus it is difficult to determine it with accuracy. In order to distinguish it from the bulk Rh_2O_3 , the ultrathin rhodium oxide film will be hereafter referred as RhO_x with $x < 2$ so as to take into account the previously proposed O–Rh–O trilayer structure [32, 40]. More about the effect of the surface RhO_x layer will be discussed in detail below.

By using a deconvolution procedure similar to that illustrated in Fig. 3, the percentage of the RhO_x film to the overall Rh 3d XPS signal can be estimated. The evolution of the RhO_x -related peak as a function of temperature for the 2 reaction mixtures ($R = 0.2$ and $R = 3.6$) is shown in Fig. 4. In reducing reaction mixture ($R = 3.6$) the oxidation of Rh follows three distinct stages as the temperature is increasing, (i) an initial low temperature region up to 90 °C where rhodium oxidation state is not influenced, (ii) a relatively slow development of an oxide film from 90 to 240 °C and (iii) a rapid decomposition of the RhO_x film from 250 to 270 °C. In case of oxidizing reaction mixture ($R = 0.2$) a clear difference can be seen. Although the ignition temperature of oxide

formation is similar, the oxide film thickness continuously grows with temperature without any evident sign of decomposition, at least up to the maximum annealing temperature (400 °C). It is interesting to note that the rate of oxide formation, thus the fraction of the RhO_x , is related mainly to the temperature and is independent of the reaction atmosphere (at least for R values up to 3.6). The fact that Rh can be oxidised even under reducing conditions has been already observed and discussed in the past during EPOC studies of ethylene oxidation on Rh/YSZ under atmospheric pressure [12, 13, 19, 20]. Pliangos et al. [19] reported that Rh is oxidized at 350 °C under reactant mixtures of $R=2.27$ and become metal at ratios $R > 4$.

By means of Eq. 1 one can estimate the evolution of the average RhO_x film thickness as a function of temperature. These values, represented in the right y-axis of Fig. 4, suggest that under our experimental conditions the RhO_x film does never exceed 0.5 nm thickness, which would correspond to a maximum of about 3 atomic layers.

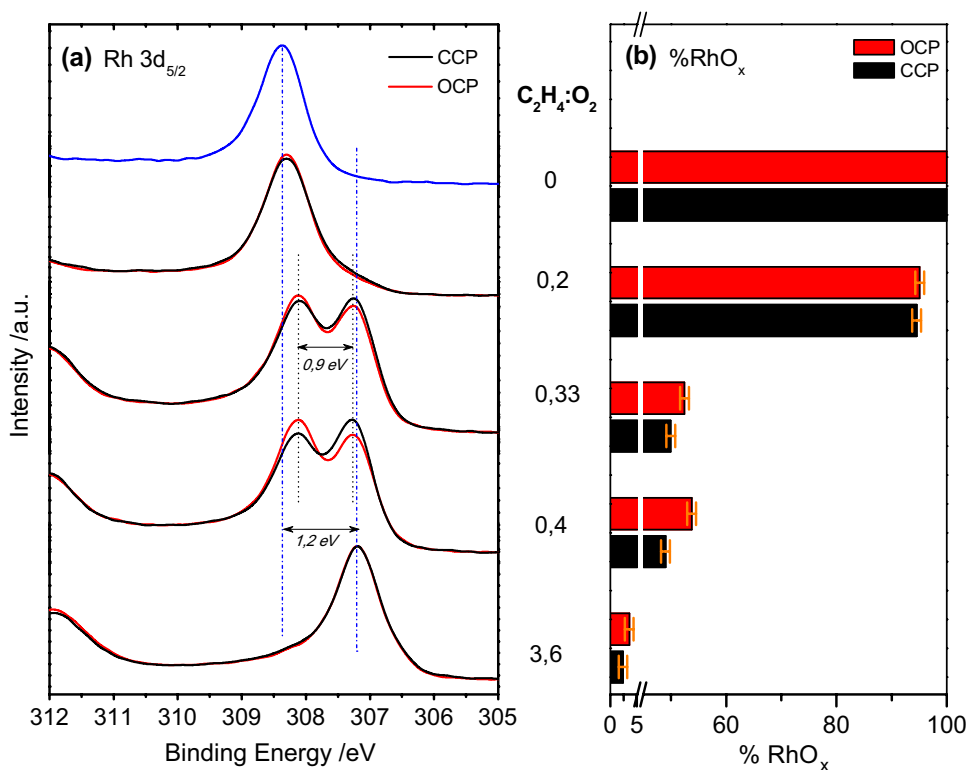
3.4 Comparison of the Rh Oxidation State Under Open and Close Circuit Conditions

The Rh $3d_{5/2}$ spectra recorded at 350 °C under 4 different $p_{(\text{C}_2\text{H}_4)}/p_{(\text{O}_2)}$ molar ratios are shown in Fig. 5a. In all cases the experiment started from a fully oxidized Rh_2O_3 electrode formed under 100% O_2 ($R=0$). As expected, Rh_2O_3 reduces gradually to metallic Rh as the reaction mixture is shifted to

more reducing compositions (mixtures more rich in ethylene). However, it seems that there is an abrupt reduction step when the reaction mixture switches from oxidative ($R=0.2$) to stoichiometric molar ratio ($R=0.33$). It is also interesting to note that reduction of Rh_2O_3 proceeds even in oxidative reactant molar ratio ($R=0.2$), as shown by the appearance of the shoulder at 307.2 eV in the Rh $3d_{5/2}$ spectra of Fig. 5a.

The influence of the applied potential ($U_{\text{WC}} = 1.5$ V) to rhodium oxidation state becomes evident by simple comparison of the Rh $3d_{5/2}$ spectra recorded in OC and CC conditions at the same reaction mixture (Fig. 5a). In order to rule out any artifacts due to possible transition states' slowly adapting to the applied conditions, care was taken that the spectra in OC and CC were recorded under identical exposure periods (20 min). To facilitate the comparison, the fraction of the RhO_x peak in the overall Rh 3d spectrum, obtained by Rh 3d peak deconvolution is shown in Fig. 5b. Apparently, the % RhO_x is systematically lower at +1.5 V conditions as compared to OC. The repeatability/reproducibility of this observation was confirmed in independent experiments starting from reduced Rh electrodes as well as, at experiments performed at 250 °C, both shown in the supporting information (Fig. S1). Therefore, although the differences in the Rh oxidation state between OC and CC conditions are subtle, they are consistent in several independent experiments and therefore are reliable. Accordingly, our results provide a direct evidence for the effect of the applied potential to the oxidation state of the Rh electrode.

Fig. 5 **a** Rh $3d_{5/2}$ NAP-XPS spectra recorded at 350 °C in various $p_{(\text{C}_2\text{H}_4)}/p_{(\text{O}_2)}$ reaction mixtures under open and close ($U_{\text{WC}} = 1.5$ V) circuit conditions. The spectra are normalized in height to facilitate the comparison, the vertical lines are present as eye guide. **b** The % RhO_x to the overall Rh 3d spectrum calculated for the spectra presented in **a**. The signal to noise ratio (S/N) of the Rh 3d spectra is about 120 suggesting that the error in the RhO_x estimation is better than 0.8%. Please note that in the case of 0 and 0.2 reaction mixtures oxidized Rh is mainly in the Rh_2O_3 state



In particular, it is shown that under anodic applied potential the Rh oxide stability decreases and the electrode is more reduced, as compared to the OC conditions.

This observation is in agreement with the sacrificial promoter model [3–8, 43] of electrochemical promotion and metal-support interactions with O^{2-} conducting supports. According to this model [3–8, 12–14], the backspillover oxide ions are less reactive to ethylene than normally chemisorbed oxygen and act as promoters by affecting the binding strength of chemisorbed oxygen and ethylene. Thus, increasing catalyst potential weakens the chemisorptive bond of atomic oxygen and causes the destabilization of rhodium oxide [44]. In our case, the anodically controlled migration (backspillover) of O^{2-} species from YSZ to the Rh/gas interface is found to decrease the amount of RhO_x in the Rh 3d peak. Less RhO_x XPS signal can be provoked by various RhO_x film changes such as, the oxide film becomes smaller in thickness, its stoichiometry changes in favour of Rh metal, or areas of metallic Rh under the RhO_x film are uncovered. Although one cannot unambiguously assign the observed changes to one of the above catalysts' features, the enhancement of metallic Rh proportion at the outermost surface layers, remains a clear indication of electrode reduction under potential. Comparison of the O 1s spectra between open and close circuit conditions did not reveal any evident differences as shown for two characteristic cases in the supporting information (Fig. S2). The difficulty to detect reactive/spillover oxygen species might reflect the fact that their concentration is very low under the employed conditions and their detection is complicated by the relatively high O 1s signal of the Rh oxide and the support.

Energy resolved depth profile NAP-XPS measurements (spectra similar to those presented in Fig. 3) suggest that in all feed mixtures RhO_x is preferentially on the surface of the electrode, while metallic Rh is located at the subsurface under the oxide film. This indicates that the reduction of Rh oxide in the reaction mixture might proceed via a mechanism where Rh is reduced on the surface and then diffuses fast in the interior of the electrode until equilibrium is established. The Rh oxidation state at the equilibrium is directly related to the redox effect of the gas mixture and temperature. The experimental confirmation of a few-atomic-layer thick RhO_x layer on the surface of the electrode under stoichiometric and moderate reducing reaction mixtures is an important new evidence that the catalytic activity of the electrode does not necessarily requires complete reduction to metallic Rh. Alternatively, as shown in Fig. 6b, a thin RhO_x surface layer can be also active for the reaction.

This observation is also supported by several previous studies on Pt-group metals, such as Ru [45], Pd [46] and Rh [35], which showed that a thin surface oxide film over a metal core, is the most reactive catalyst formulation for catalytic CO oxidation. We also recall that formation of different

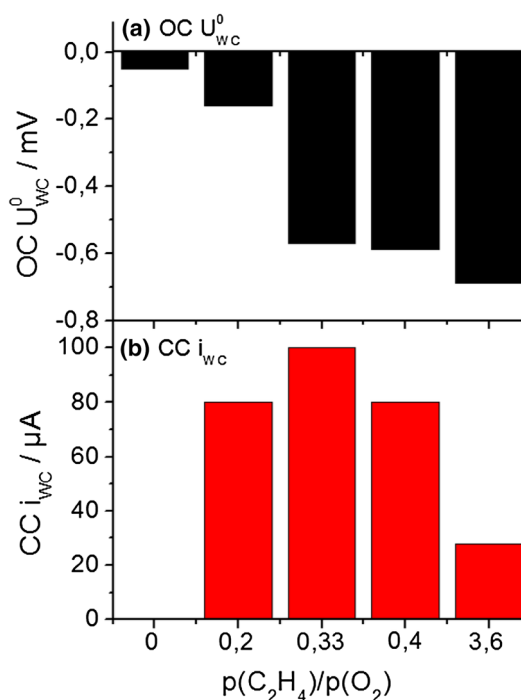


Fig. 6 **a** The cell voltage between the working (Rh) and counter (Au) electrodes measured at 350 °C and at OC for various $p(C_2H_4)/p(O_2)$ reaction mixtures. **b** The cell current measured under identical pressure temperature and gas mixture conditions under 1.5 V applied potential between Rh and Au electrodes

Ru surface oxides was suggested to play an important role in the catalytic behavior of Ru electrodes in fuel cell applications [47, 48]. Typically, surface oxides are described as a distorted few layer oxide phase on the top of the metal. Their stoichiometry may change dynamically with the reaction conditions and depends on the reduction–oxidation equilibrium maintained by the reactants partial pressure. In general, they are considered to be oxygen deficient as compared to the stoichiometric oxide. In addition, in most cases the characteristic spectral features in photoemission differ from those of the stoichiometric oxide phase, as clearly observed here.

The potential of the electrode was monitored in conjunction with the surface characterization by on line electrical measurements of the cell. Figure 6a shows the modification of the potential of Rh film (working electrode) relative to the gold counter electrode at the examined reaction feed mixtures. An abrupt decrease of the catalyst potential of about 400 mV is observed at stoichiometric molar ratio ($R=0.33$) while the potential further drops by about 100 mV at reducing molar ratios. The observed potential values are in the same order of magnitude with previously reported values in EPOC studies of ethylene oxidation on Rh/YSZ under atmospheric pressure [12, 13, 19, 20]. However, since we have not used a reference electrode in our setup, the reported

potentials cannot be directly established with those of other works.

Correlation of the Rh oxidation state with the potential drop at open circuit indicates that the reduction of the surface oxide (observed at highly reducing molar ratios) has a much weaker influence on the OC as compared to the reduction of the interior of the Rh electrode (ignited at stoichiometric potential). Figure 6b shows the current flowing between the rhodium and gold electrodes when a constant anodic potential of +1.5 V is applied between them at the examined reaction mixtures. The current reaches a maximum value of 100 μA at molar ratio $R=0.33$ while it decreases at higher ratios. This observation confirms that in the range of feed ratios in which the RhO_x surface film is stabilized (stoichiometric and mild reducing reactant mixtures) the cell current is maximum.

4 Conclusions

In this work we monitored the surface of Rh/YSZ electrodes during ethylene oxidation under open circuit condition and anodic polarization in various $p_{(\text{C}_2\text{H}_4)}/p_{(\text{O}_2)}$ mixtures. We demonstrate the dynamic response of the Rh oxidation state which is determined by the composition of the reaction mixture. We also provide direct spectroscopic evidences that anodic polarization, i.e. oxygen ion supply to the preoxidised Rh catalytic surface, can change the surface oxidation state by promoting reduction of oxidized Rh to metallic in agreement with the sacrificial promoter model of electrochemical promotion and metal-support interactions with O^{2-} conducting supports. One of the most interesting results of this study is the observation of the existence of a surface rhodium oxide layer, RhO_x ($x < 2$), stabilized under moderately reducing mixtures. The surface oxide is likely to have different catalytic properties than the bulk Rh_2O_3 phase due to its limited thickness and the close proximity to the metallic Rh subsurface. These partially reduced catalytic centres may have a key role to the pronounced catalytic performance of Rh/YSZ catalysts under electropromoted conditions.

Acknowledgements We thank AC department of FHI and in particular M. Hävecker and A. Knop-Gericke for the opportunity to use the ISS beamline and HZB for the allocation of synchrotron radiation beamtime. We acknowledge the support of Dr. T. Dintzer for the SEM images and Dr. Y.T. Law during the beamtime measurements.

References

- Ladas S, Kennou S, Bebelis S, Vayenas CG (1993) Origin of non-faradaic electrochemical modification of catalytic activity. *J Phys Chem* 97:8845–8848. <https://doi.org/10.1021/j100137a004>
- Vayenas CG (2013) Promotion, electrochemical promotion and metal-support interactions: their common features. *Catal Lett* 143:1085–1097. <https://doi.org/10.1007/s10562-013-1128-x>
- Vayenas CG, Bebelis S, Pliangos C et al (2001) Electrochemical activation of catalysis: promotion, electrochemical promotion, and metal-support interactions. <https://doi.org/10.1007/b115566>
- Vayenas CG, Koutsodontis CG (2008) Non-faradaic electrochemical activation of catalysis. *J Chem Phys.* <https://doi.org/10.1063/1.2824944>
- Katsaounis A (2010) Recent developments and trends in the electrochemical promotion of catalysis (EPOC). *J Appl Electrochem* 40(5):885–902
- Vayenas CG (2011) Bridging electrochemistry and heterogeneous catalysis. *J Solid State Electrochem* 15:1425–1435. <https://doi.org/10.1007/s10008-011-1336-5>
- Tsiplakides D, Balomenou S (2009) Milestones and perspectives in electrochemically promoted catalysis. *Catal Today* 146:312–318. <https://doi.org/10.1016/j.cattod.2009.05.015>
- Vernoux P, Lizarraga L, Tsampas MN et al (2013) Ionically conducting ceramics as active catalyst supports. *Chem Rev* 113:8192–8260. <https://doi.org/10.1021/cr4000336>
- Van Herle J, McEvoy a J (1994) Oxygen diffusion through silver cathodes for solid oxide fuel cells. *J Phys Chem Solids* 55:339–347. [https://doi.org/10.1016/0022-3697\(94\)90230-5](https://doi.org/10.1016/0022-3697(94)90230-5)
- Adler SB (2004) Factors governing oxygen reduction in solid oxide fuel cell cathodes. *Chem Rev* 104:4791–4843. <https://doi.org/10.1021/cr020724o>
- Fleig J, Jamnik J (2005) Work function changes of polarized electrodes on solid electrolytes. *J Electrochem Soc* 152:E138. <https://doi.org/10.1149/1.1862479>
- Baranova EA, Thursfield A, Brosda S et al (2005) Electrochemically induced oscillations of C_2H_4 oxidation over thin sputtered Rh catalyst films. *Catal Lett* 105:15–21. <https://doi.org/10.1007/s10562-005-7999-8>
- Baranova EA, Thursfield A, Brosda S et al (2005) Electrochemical promotion of ethylene oxidation over Rh catalyst thin films sputtered on YSZ and TiO_2/YSZ supports. *J Electrochem Soc* 152:E40–E49. <https://doi.org/10.1149/1.1839511>
- Brosda S, Badas T, Vayenas CG (2011) Study of the mechanism of the electrochemical promotion of Rh/YSZ catalysts for C_2H_4 oxidation via AC impedance spectroscopy. *Top Catal* 54:708–717. <https://doi.org/10.1007/s11244-011-9679-9>
- De Lucas-Consuegra A, González-Cobos J, Carcelén V et al (2013) Electrochemical promotion of Pt nanoparticles dispersed on a diamond-like carbon matrix: a novel electrocatalytic system for H_2 production. *J Catal* 307:18–26. <https://doi.org/10.1016/j.jcat.2013.06.012>
- Fortunato MA, Princivalle A, Capdeillacre C et al (2014) Role of lattice oxygen in the propane combustion over Pt/Yttria-stabilized zirconia: isotopic studies. *Top Catal* 57:1277–1286. <https://doi.org/10.1007/s11244-014-0293-5>
- Hajar YM, Patel KD, Tariq U, Baranova EA (2017) Functional equivalence of electrochemical promotion and metal support interaction for Pt and RuO_2 nanoparticles. *J Catal* 352:42–51. <https://doi.org/10.1016/j.jcat.2017.05.001>
- Vayenas CG, Bebelis S, Ladas S (1990) Dependence of catalytic rates on catalyst work function. *Nature* 343:625–627. <https://doi.org/10.1038/343625a0>
- Pliangos C, Yentekakis IV, Verykios XE, Vayenas CG (1995) Non-faradaic electrochemical modification of catalytic activity. 8. Rh-catalyzed C_2H_4 oxidation. *J Catal* 154:124–136. <https://doi.org/10.1006/jcat.1995.1154>
- Pliangos C, Yentekakis IV, Papadakis VG et al (1997) Support-induced promotional effects on the activity of automotive exhaust catalysts: 1. The case of oxidation of light hydrocarbons (C_2H_4).

- Appl Catal B Environ 14:161–173. [https://doi.org/10.1016/S0926-3373\(97\)00020-9](https://doi.org/10.1016/S0926-3373(97)00020-9)
21. Neophytides SGG, Zafeiratos S, Kennou S (2000) XPS characterization of the electrochemically generated O species on a Au electrode evaporated on Y₂O₃-stabilized ZrO₂ (100). *Solid State Ionics* 136:801–806. [https://doi.org/10.1016/S0167-2738\(00\)00542-7](https://doi.org/10.1016/S0167-2738(00)00542-7)
 22. Stoerzinger KA, Hong WT, Crumlin EJ et al (2015) Insights into electrochemical reactions from ambient pressure photoelectron spectroscopy. *Acc Chem Res* 48:2976–2983. <https://doi.org/10.1021/acs.accounts.5b00275>
 23. Paloukis F, Papazisi KM, Balomenou SP et al (2017) In situ X-ray photoelectron spectroscopy study of complex oxides under gas and vacuum environments. *Appl Surf Sci* 423:1176–1181. <https://doi.org/10.1016/j.apsusc.2017.06.219>
 24. Toghan A, Arrigo R, Knop-Gericke A, Imbihl R (2012) Ambient pressure X-ray photoelectron spectroscopy during electrochemical promotion of ethylene oxidation over a bimetallic Pt-Ag/YSZ catalyst. *J Catal* 296:99–109. <https://doi.org/10.1016/j.jcat.2012.09.006>
 25. Carberry JJ (1976) *Chemical and catalytic reaction engineering*. McGraw-Hill, New York
 26. Knop-Gericke A, Kleimenov E, Hävecker M et al (2009) X-ray photoelectron spectroscopy for investigation of heterogeneous catalytic processes. *Adv Catal* 52:213–272. [https://doi.org/10.1016/S0360-0564\(08\)00004-7](https://doi.org/10.1016/S0360-0564(08)00004-7)
 27. Papaefthimiou V, Shishkin M, Niakolas DK et al (2013) On the active surface state of nickel-ceria solid oxide fuel cell anodes during methane electrooxidation. *Adv Energy Mater* 3:762–769. <https://doi.org/10.1002/aenm.201200727>
 28. Papaefthimiou V, Niakolas DK, Paloukis F et al (2017) Operando observation of nickel/ceria electrode surfaces during intermediate temperature steam electrolysis. *J Catal* 352:305–313. <https://doi.org/10.1016/j.jcat.2017.06.005>
 29. Tanuma S, Powell CJ, Penn DR (1993) Calculations of electron inelastic mean free paths. *Surf Interface Anal* 21:165–176. <https://doi.org/10.1002/sia.740210302>
 30. Yeh JJ, Lindau I (1985) Atomic subshell photoionization cross sections and asymmetry parameters: $1 < Z < 103$. *At Data Nucl Data Tables* 32:1–155. [https://doi.org/10.1016/0092-640X\(85\)90016-6](https://doi.org/10.1016/0092-640X(85)90016-6)
 31. Powell CJJ, Jablonski A (2010) Progress in quantitative surface analysis by X-ray photoelectron spectroscopy: current status and perspectives. *J Electron Spectrosc Relat Phenom* 178:331–346. <https://doi.org/10.1016/j.elspec.2009.05.004>
 32. Blomberg S, Lundgren E, Westerström R et al (2012) Structure of the Rh₂O₃(0001) surface. *Surf Sci* 606:1416–1421. <https://doi.org/10.1016/j.susc.2012.05.004>
 33. Blomberg S, Westerström R, Martin NM et al (2014) A high pressure X-ray photoelectron spectroscopy study of oxidation and reduction of Rh(100) and Rh nanoparticles. *Surf Sci* 628:153–158. <https://doi.org/10.1016/j.susc.2014.06.009>
 34. Kibis LS, Stadnichenko AI, Koscheev SV et al (2016) XPS study of nanostructured rhodium oxide film comprising Rh⁴⁺ species. *J Phys Chem C* 120:19142–19150. <https://doi.org/10.1021/acs.jpcc.6b05219>
 35. Grass ME, Zhang Y, Butcher DR et al (2008) A reactive oxide overlayer on rhodium nanoparticles during CO oxidation and its size dependence studied by in situ ambient-pressure X-ray photoelectron spectroscopy. *Angew Chem Int Ed* 47:8893–8896. <https://doi.org/10.1002/anie.200803574>
 36. Dri C, Africh C, Esch F et al (2006) Initial oxidation of the Rh(110) surface: ordered adsorption and surface oxide structures. *J Chem Phys*. <https://doi.org/10.1063/1.2345058>
 37. Marot L, Mathys D, Temmerman G, De Oelhafen P (2008) Characterization of sub-stoichiometric rhodium oxide deposited by magnetron sputtering. *Surf Sci* 602:3375–3380. <https://doi.org/10.1016/j.susc.2008.09.012>
 38. Paloukis F, Papazisi KM, Dintzer T et al (2017) Insights into the surface reactivity of Cermet and Perovskite electrodes in oxidizing, reducing, and humid environments. *ACS Appl Mater Interfaces* 9:25265–25277. <https://doi.org/10.1021/acsami.7b05721>
 39. Parmigiani F, Depero LE, Sangaletti L, Samoggia G (1993) An XPS study of yttria-stabilised zirconia single crystals. *J Electron Spectrosc Relat Phenomena* 63:1–10. [https://doi.org/10.1016/0368-2048\(93\)85010-1](https://doi.org/10.1016/0368-2048(93)85010-1)
 40. Gustafson J, Mikkelsen A, Borg M et al (2004) Self-limited growth of a thin oxide layer on Rh(111). *Phys Rev Lett* 92:126101–126102. <https://doi.org/10.1103/PhysRevLett.92.126102>
 41. Doh WHWH, Papaefthimiou V, Dintzer T et al (2014) Synchrotron radiation X-ray photoelectron spectroscopy as a tool to resolve the dimensions of spherical core/shell nanoparticles. *J Phys Chem C* 118:26621–26628. <https://doi.org/10.1021/jp508895u>
 42. Mittendorfer F (2010) Low-dimensional surface oxides in the oxidation of Rh particles. *J Phys Condens Matter* 22:393001. <https://doi.org/10.1088/0953-8984/22/39/393001>
 43. Katsaounis A, Nikopoulou Z, Verykios XE, Vayenas CG (2004) Comparative isotope-aided investigation of electrochemical promotion and metal-support interactions: 2. CO oxidation by 18O₂ on electropromoted Pt films deposited on YSZ and on nanodispersed Pt/YSZ catalysts. *J Catal* 226:197–209. <https://doi.org/10.1016/j.jcat.2004.05.009>
 44. Vayenas CG, Bebelis S, Yentekakis IV, Lintz HG (1992) Non-faradaic electrochemical modification of catalytic activity: a status report. *Catal Today* 11:303–438. [https://doi.org/10.1016/0920-5861\(92\)80002-5](https://doi.org/10.1016/0920-5861(92)80002-5)
 45. Assmann J, Crihan D, Knapp M et al (2005) Understanding the structural deactivation of ruthenium catalysts on an atomic scale under both oxidizing and reducing conditions. *Angew Chem Int Ed* 44:917–920. <https://doi.org/10.1002/anie.200461805>
 46. Hendriksen BLM, Frenken JWM (2002) CO oxidation on Pt(110): scanning tunneling microscopy inside a high-pressure flow reactor. *Phys Rev Lett*. <https://doi.org/10.1103/PhysRevLett.89.046101>
 47. Danilovic N, Subbaraman R, Chang KC et al (2014) Using surface segregation to design stable Ru-Ir oxides for the oxygen evolution reaction in acidic environments. *Angew Chem Int Ed* 53:14016–14021. <https://doi.org/10.1002/anie.201406455>
 48. Saveleva VA, Wang L, Luo W et al (2016) Uncovering the stabilization mechanism in bimetallic ruthenium-iridium anodes for proton exchange membrane electrolyzers. *J Phys Chem Lett* 7:3240–3245. <https://doi.org/10.1021/acs.jpcclett.6b01500>